Supplemental Information

Supplemental methods

Normalized difference vegetation index (NDVI; Supplemental Equation 1) correlates with vegetation density, canopy cover, and leaf area index (1). Normalized difference moisture index (NDMI; Supplemental Equation 2) correlates with similar vegetation characteristics as NDVI, but doesn't saturate at high levels of foliar biomass (2). Normalized burn ratio (NBR; Supplemental Equation 3) and normalized burn ratio version 2 (NBR2; Supplemental Equation 4) respond strongly to fire effects on vegetation (4–8).

(1) $ndvi = (nir - red)/(nir + red)$

(2) $ndmi = (nir - swir1)/(nir + swir1)$

(3) $nbr = (nir - swir2)/(nir + swir2)$

(4) $nbr2 = (swir1 - swir2)/(swir1 + swir2)$

Where nir is the near infrared band (band 4 on Landsat 4, 5, and 7; band 5 on Landsat 8) and red is the red band (band 3 on Landsat 4, 5, and 7; band 4 on Landsat 8), $swir1$ is the first short wave infrared band (band 5 on Landsat 4, 5, and 7; band 4 on Landsat 8), $swir2$ is the second short wave infrared band (band 7 on Landsat 4, 5, 7, and 8)

We calculated the delta severity indices (dNBR, dNBR2, dNDVI) by subtracting the respective postfire indices from the prefire indices (NBR, NBR2, and NDVI) without multiplying by a rescaling constant (e.g., we did not multiply the result by 1000 as in (9); Supplemental Equation 5). Following (10), we chose not to correct the delta indices using a phenological offset value (typically calculated as the delta index in homogeneous forest patch outside of the fire perimeter), as our approach implicitly accounts for phenology by incorporating multiple cloud-free images across the same time window both before the fire and one year later.

(5) $dI = I_{\text{prefire}} - I_{\text{postfire}}$

We calculated the relative delta severity indices, RdNBR and RdNDVI, by scaling the respective delta indices (dNBR and dNDVI) from Supplemental Equation 6 by a square root transformation of the absolute value of the prefire index:

(6) $RdI = \dfrac{dI}{\sqrt{|I_{\text{prefire}}|}}$

We calculated the relative burn ratio (RBR) following **???** using Supplemental Equation 7:

(7) $RBR = \dfrac{dNBR}{NBR_{\text{prefire}} + 1.001}$

1

We used the digital elevation model to calculate the potential annual heat load (Supplemental Equation 8 at each pixel, which is an integrated measure of latitude, slope, and a folding transformation of aspect about the northeast-southwest line, such that northeast becomes 0 radians and southwest becomes π radians (11, 12):

$$aspect_{folded} = |\pi - |aspect - \frac{5\pi}{4}||$$

$$log(pahl) = \begin{aligned}&-1.467+\\&1.582 * cos(latitude)cos(slope)-\\&1.5 * cos(aspect_{folded})sin(slope)sin(latitude)-\\&0.262 * sin(lat)sin(slope)+\\&0.607 * sin(aspect_{folded})sin(slope)\end{aligned} \quad (8)$$

Where $pahl$ is the potential annual heat load, $aspect_{folded}$ is a transformation of aspect in radians, and both *latitude* and *slope* are extracted from a digital elevation model with units of radians.

Supplemental figures and tables

Supplemental Table 1: Comparison of models used to validate and calibrate remotely sensed wildfire severity with ground-based composite burn index (CBI) severity sorted in descending order by the R^2 value from a 5-fold cross validation. A total of 56 models were tested representing all possible combinations of 7 different measures of wildfire severity (RBR, dNBR, dNBR2, RdNBR, RdNBR2, dNDVI, and RdNDVI), 4 different time windows in which Landsat imagery was acquired and summarized with a median reducer on a pixel-by-pixel basis (16 days, 32 days, 48 days, and 64 days), and two different interpolation methods (bilinear and bicubic). The three parameters (β_0, β_1, and β_2) from the nonlinear model fit described in Eq. 1 are reported. For each model, the value of the remotely sensed wildfire severity measurement corresponding to the lower bounds of 3 commonly used categories of severity are reported ('low' corresponds to a CBI value of 0.1, 'mod' corresponds to a CBI value of 1.25, and 'high' corresponds to a CBI value of 2.25)

Rank	Severity measure	Time window	Interpolation	k-fold R^2	β_0	β_1	β_2	low	mod	high
1	RBR	48	bicubic	0.82	0.014	0.028	1.001	0.045	0.113	0.282
2	RdNBR	32	bilinear	0.813	-0.483	3.061	0.857	2.852	8.45	20.56
3	RdNDVI	48	bilinear	0.809	-2.144	3.273	0.609	1.335	4.867	10.75
4	RBR	32	bilinear	0.807	0.014	0.029	0.985	0.046	0.113	0.28
5	RdNDVI	64	bicubic	0.805	-2.524	3.57	0.59	1.263	4.936	10.93
6	RBR	64	bicubic	0.805	0.016	0.027	1.01	0.046	0.113	0.283
7	RdNDVI	32	bicubic	0.803	-2.737	3.308	0.619	0.782	4.436	10.59
8	RBR	64	bilinear	0.802	0.017	0.027	1.003	0.047	0.113	0.279
9	RdNDVI	32	bilinear	0.801	-2.531	3.176	0.624	0.849	4.393	10.39

Rank	Severity measure	Time window	Interpolation	k-fold R^2	β_0	β_1	β_2	low	mod	high
10	RdNDVI	48	bicubic	0.797	-2.623	3.624	0.587	1.22	4.922	10.94
11	RdNDVI	64	bilinear	0.796	-2.14	3.287	0.607	1.353	4.876	10.73
12	RdNBR	64	bilinear	0.792	-0.42	3.031	0.862	2.884	8.483	20.66
13	RBR	48	bilinear	0.791	0.017	0.027	1.006	0.047	0.112	0.277
14	RBR	32	bicubic	0.79	0.013	0.029	0.994	0.045	0.114	0.284
15	RdNBR	48	bicubic	0.785	-0.858	3.219	0.852	2.647	8.476	21.02
16	RBR	16	bilinear	0.781	0.021	0.026	1.016	0.05	0.114	0.278
17	RdNBR	32	bicubic	0.776	-0.954	3.34	0.841	2.679	8.602	21.2
18	dNDVI	32	bicubic	0.776	-0.058	0.073	0.65	0.02	0.106	0.257
19	dNBR	48	bicubic	0.775	0.03	0.035	1.069	0.068	0.161	0.413
20	RdNBR	16	bilinear	0.774	0.279	2.518	0.909	3.037	8.119	19.73
21	dNDVI	32	bilinear	0.772	-0.053	0.07	0.656	0.022	0.105	0.252
22	dNDVI	48	bicubic	0.772	-0.055	0.081	0.613	0.031	0.119	0.267
23	dNBR	32	bilinear	0.77	0.029	0.036	1.048	0.069	0.163	0.41
24	RdNBR2	64	bicubic	0.766	2.102	0.416	1.24	2.572	4.059	8.861
25	dNBR	32	bicubic	0.764	0.028	0.036	1.057	0.068	0.163	0.417
26	dNDVI	48	bilinear	0.762	-0.044	0.073	0.637	0.034	0.118	0.262
27	RBR	16	bicubic	0.761	0.021	0.026	1.028	0.049	0.114	0.281
28	dNBR	16	bilinear	0.76	0.033	0.036	1.048	0.073	0.167	0.417
29	RdNBR2	32	bilinear	0.759	1.435	0.625	1.1	2.132	3.906	8.861
30	RdNBR	16	bicubic	0.758	0.37	2.446	0.926	3.053	8.149	20
31	RdNBR2	32	bicubic	0.754	1.426	0.601	1.125	2.098	3.876	8.975
32	dNBR	64	bicubic	0.753	0.033	0.033	1.086	0.07	0.161	0.413
33	dNBR	64	bilinear	0.751	0.035	0.033	1.08	0.071	0.161	0.406
34	RdNBR2	48	bicubic	0.751	1.835	0.46	1.209	2.354	3.919	8.818
35	dNBR	48	bilinear	0.748	0.035	0.033	1.076	0.071	0.161	0.405
36	RdNDVI	16	bilinear	0.747	-0.983	2.503	0.678	1.695	4.856	10.52
37	dNDVI	64	bicubic	0.746	-0.055	0.082	0.609	0.032	0.12	0.266
38	dNDVI	64	bilinear	0.741	-0.046	0.075	0.627	0.034	0.118	0.261
39	RdNBR2	48	bilinear	0.737	1.802	0.497	1.174	2.361	3.956	8.766

| Rank	Severity measure	Time window	Interpolation	k-fold R^2	β_0	β_1	β_2	low	mod	high
40	RdNBR	64	bicubic	0.737	-1.448	3.651	0.819	2.515	8.717	21.61
41	RdNBR2	64	bilinear	0.735	2.027	0.451	1.204	2.536	4.06	8.801
42	dNBR	16	bicubic	0.729	0.032	0.036	1.058	0.072	0.168	0.423
43	dNBR2	32	bilinear	0.727	0.026	0.009	1.149	0.035	0.062	0.14
44	dNDVI	16	bicubic	0.726	-0.03	0.065	0.674	0.04	0.121	0.267
45	RdNDVI	16	bicubic	0.725	-1.248	2.681	0.665	1.618	4.908	10.72
46	dNBR2	32	bicubic	0.715	0.025	0.008	1.177	0.035	0.061	0.142
47	dNBR2	64	bilinear	0.714	0.036	0.006	1.283	0.043	0.064	0.137
48	dNDVI	16	bilinear	0.707	-0.023	0.06	0.689	0.042	0.12	0.261
49	dNBR2	48	bilinear	0.686	0.033	0.006	1.248	0.04	0.063	0.137
50	RdNBR2	16	bilinear	0.682	1.928	0.465	1.189	2.452	3.983	8.676
51	dNBR2	16	bilinear	0.662	0.03	0.009	1.138	0.04	0.066	0.143
52	RdNBR2	16	bicubic	0.654	1.871	0.467	1.198	2.398	3.96	8.792
53	dNBR2	16	bicubic	0.635	0.029	0.009	1.156	0.039	0.066	0.145
54	RdNBR	48	bilinear	0.63	-3.445	5.132	0.724	2.072	9.235	22.7
55	dNBR2	48	bicubic	0	0.033	0.006	1.284	0.04	0.062	0.138
56	dNBR2	64	bicubic	0	0.037	0.005	1.313	0.043	0.064	0.139

Supplemental Table 2: Model parameter estimates for different neighborhood sizes. Values represent the mean parameter estimates with 95% credible intervals in parentheses.

Coefficient	90m x 90m neighborhood	150m x 150m neighborhood	210m x 210m neighborhood	270m x 270m neighborhood
β_0	-2.415 (-2.588, -2.255)	-2.432 (-2.605, -2.271)	-2.447 (-2.619, -2.279)	-2.45 (-2.618, -2.288)
$\beta_{\text{nbhd\_stdev\_NDVI}}$	-0.208 (-0.247, -0.17)	-0.212 (-0.255, -0.17)	-0.203 (-0.248, -0.158)	-0.195 (-0.242, -0.148)
$\beta_{\text{prefire\_NDVI}}$	1.044 (0.911, 1.174)	1.13 (1.028, 1.229)	1.141 (1.057, 1.222)	1.132 (1.056, 1.209)

Coefficient	90m x 90m neighborhood	150m x 150m neighborhood	210m x 210m neighborhood	270m x 270m neighborhood
β_{fm100}	-0.569 (-0.71, -0.423)	-0.564 (-0.709, -0.419)	-0.561 (-0.697, -0.428)	-0.565 (-0.712, -0.422)
β_{pahl}	0.239 (0.208, 0.271)	0.238 (0.205, 0.269)	0.239 (0.207, 0.269)	0.24 (0.209, 0.272)
$\beta_{\text{topographic\_roughness}}$	-0.01 (-0.042, 0.022)	-0.006 (-0.039, 0.027)	-0.002 (-0.037, 0.032)	-0.002 (-0.036, 0.033)
$\beta_{\text{nbhd\_mean\_NDVI}}$	-0.14 (-0.278, 0.002)	-0.265 (-0.381, -0.148)	-0.293 (-0.392, -0.193)	-0.293 (-0.389, -0.198)
$\beta_{\text{nbhd\_stdev\_NDVI*prefire\_NDVI}}$	0.125 (0.029, 0.218)	0.06 (-0.013, 0.135)	0.022 (-0.045, 0.09)	0.009 (-0.054, 0.072)
$\beta_{\text{nbhd\_stdev\_NDVI*nbhd\_mean\_NDVI}}$	-0.129 (-0.223, -0.034)	-0.078 (-0.151, -0.006)	-0.03 (-0.095, 0.035)	-0.006 (-0.068, 0.054)
$\beta_{\text{nbhd\_stdev\_NDVI*fm100}}$	-0.037 (-0.081, 0.006)	-0.035 (-0.078, 0.01)	-0.03 (-0.076, 0.014)	-0.023 (-0.07, 0.023)
$\beta_{\text{nbhd\_mean\_NDVI*prefire\_NDVI}}$	-0.573 (-0.62, -0.526)	-0.564 (-0.612, -0.516)	-0.549 (-0.596, -0.502)	-0.537 (-0.587, -0.49)
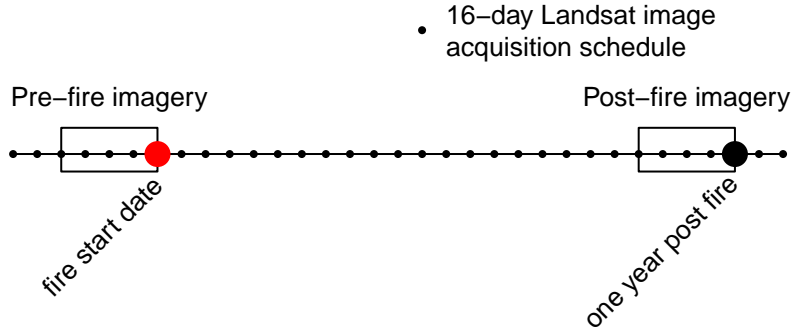
Supplemental Figure 1: Schematic for how Landsat imagery was assembled in order to make comparisons between pre- and post-fire conditions. This schematic depicts a 64-day window of image collation prior to the fire which comprise the pre-fire image collection. A similar, 64-day window collection of imagery is assembled one year after the pre-fire image collection.
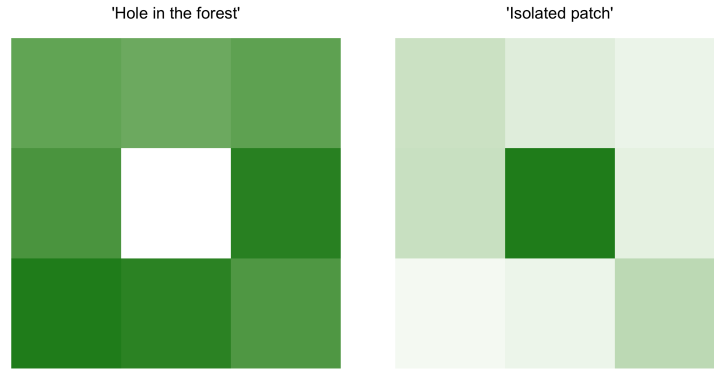
Supplemental Figure 2: Conceptual diagram of 'decoupling' that sometimes occurs between the central pixel NDVI and the neighborhood mean NDVI. In each of these scenarios, our model results suggest that the probability that the central pixel burns at high severity is higher than expected given the additive effect of the covariates. The left panel depicts the "hole in the forest" decoupling, which occurs more frequently, and the right panel depicts the "isolated patch" decoupling.

References

1. Rouse W, Haas RH, Deering W, Schell JA (1973) *MONITORING THE VERNAL ADVANCEMENT AND RETROGRADATION (GREEN WAVE EFFECT) OF NATURAL VEGETATION* (Goddard Space Flight Center, Greenbelt, MD, USA).

2. Gao B-c (1996) NDWIA normalized difference water index for remote sensing of vegetation liquid water from space. *Remote Sensing of Environment* 58(3):257–266.

3. Huesca M, García M, Roth KL, Casas A, Ustin SL (2016) Canopy structural attributes derived from AVIRIS imaging spectroscopy data in a mixed broadleaf/conifer forest. *Remote Sensing of Environment*

44 182:208–226.

45 4. García ML, Caselles V (1991) Mapping burns and natural reforestation using thematic Mapper data.
46 *Geocarto International* 6(1):31–37.

47 5. Key CH, Benson NC (2006) Landscape Assessment (LA). 55.

48 6. USGS (2017) Landsat 8 Surface Reflectance Code (LASRC) Product Guide. 40.

49 7. USGS (2017) Landsat 4-7 Surface Reflectance (LEDAPS) Product Guide. 41.

50 8. Hawbaker TJ, et al. (2017) Mapping burned areas using dense time-series of Landsat data. *Remote*
51 *Sensing of Environment* 198:504–522.

52 9. Miller JD, Thode AE (2007) Quantifying burn severity in a heterogeneous landscape with a relative version
53 of the delta Normalized Burn Ratio (dNBR). *Remote Sensing of Environment* 109(1):66–80.

54 10. Reilly MJ, et al. (2017) Contemporary patterns of fire extent and severity in forests of the Pacific
55 Northwest, USA (1985-2010). *Ecosphere* 8(3):e01695.

56 11. McCune B, Keon D (2002) Equations for potential annual direct incident radiation and heat load. *Journal*
57 *of Vegetation Science* 13(4):603–606.

58 12. McCune B (2007) Improved estimates of incident radiation and heat load using non- parametric regression
59 against topographic variables. *Journal of Vegetation Science* 18(5):751–754.